



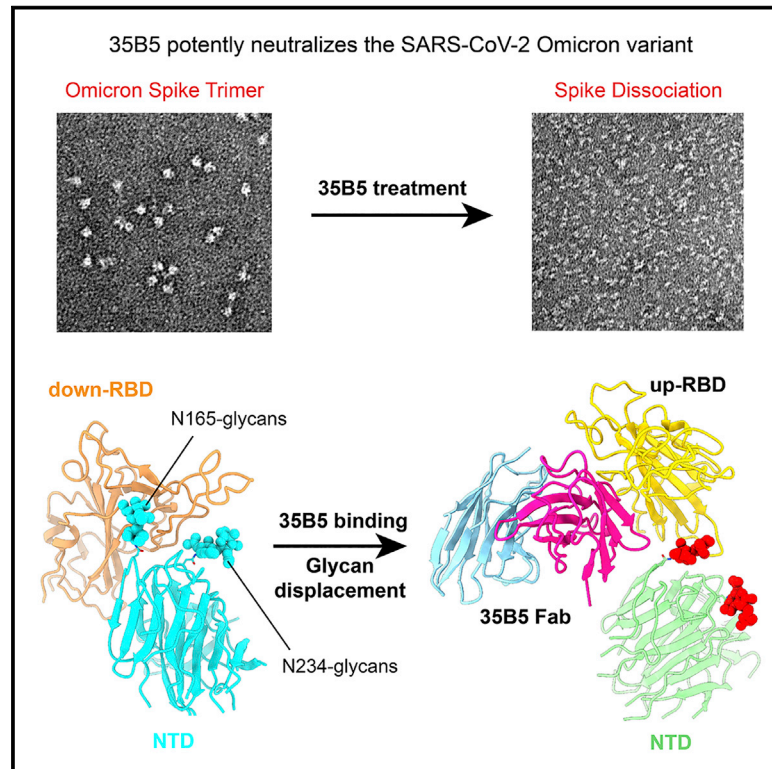
Since January 2020 Elsevier has created a COVID-19 resource centre with free information in English and Mandarin on the novel coronavirus COVID-19. The COVID-19 resource centre is hosted on Elsevier Connect, the company's public news and information website.

Elsevier hereby grants permission to make all its COVID-19-related research that is available on the COVID-19 resource centre - including this research content - immediately available in PubMed Central and other publicly funded repositories, such as the WHO COVID database with rights for unrestricted research re-use and analyses in any form or by any means with acknowledgement of the original source. These permissions are granted for free by Elsevier for as long as the COVID-19 resource centre remains active.

# Cell Host & Microbe

## 35B5 antibody potently neutralizes SARS-CoV-2 Omicron by disrupting the N-glycan switch via a conserved spike epitope

### Graphical abstract



### Authors

Xiaofei Wang, Xiangyu Chen, Jiaxing Tan, ..., Zhiwei Chen, Lilin Ye, Yongqun Zhu

### Correspondence

dengkai6@mail.sysu.edu (K.D.),  
zchenai@hku.hk (Z.C.),  
yelilinlcmv@tmmu.edu.cn (L.Y.),  
zhuyongqun@zju.edu.cn (Y.Z.)

### In brief

Wang, Chen, et al. describe an RBD-targeting monoclonal antibody, 35B5, that potently neutralizes the SARS-CoV-2 Omicron variant. 35B5 neutralizes with nanomolar efficacy by targeting an invariant epitope, resulting in the displacement of the conserved N-glycan switch from the RBD.

### Highlights

- 35B5 antibody exhibits nanomolar neutralizing efficacy to SARS-CoV-2 Omicron
- 35B5 targets the Omicron RBD via an invariant epitope
- The 35B5 epitope is essential for ACE2 binding and RBD conformational dynamics
- 35B5 displaces the conserved N-glycan switch from the RBD

Short article

# 35B5 antibody potently neutralizes SARS-CoV-2 Omicron by disrupting the N-glycan switch via a conserved spike epitope

Xiaofei Wang,<sup>1,2,10</sup> Xiangyu Chen,<sup>3,4,10</sup> Jiaying Tan,<sup>1,2</sup> Shuai Yue,<sup>5</sup> Runhong Zhou,<sup>6</sup> Yan Xu,<sup>1,2</sup> Yao Lin,<sup>5</sup> Yang Yang,<sup>3</sup> Yan Zhou,<sup>7,8</sup> Kai Deng,<sup>9,\*</sup> Zhiwei Chen,<sup>6,\*</sup> Lilin Ye,<sup>5,\*</sup> and Yongqun Zhu<sup>1,2,8,11,\*</sup>

<sup>1</sup>Department of Gastroenterology of the Second Affiliated Hospital, School of Medicine and Life Sciences Institute, Zhejiang University, Hangzhou 310058, China

<sup>2</sup>MOE Laboratory for Biosystems Homeostasis and Protection, Life Sciences Institute, Zhejiang University, Hangzhou, Zhejiang 310058, China

<sup>3</sup>School of Laboratory Medicine and Biotechnology, Southern Medical University, Guangzhou, Guangdong 510515, China

<sup>4</sup>Institute of Cancer, Xinqiao Hospital, Third Military Medical University, Chongqing 400038, China

<sup>5</sup>Institute of Immunology, PLA, Third Military Medical University, Chongqing 400038, China

<sup>6</sup>AIDS Institute and Department of Microbiology, State Key Laboratory of Emerging Infectious Diseases, Li Ka Shing Faculty of Medicine, University of Hong Kong, Pokfulam, Hong Kong Special Administrative Region, China

<sup>7</sup>Institute of Microbiology, Zhejiang University, Hangzhou, Zhejiang 310058, China

<sup>8</sup>Sir Run Run Shaw Hospital, Zhejiang University School of Medicine, Hangzhou, Zhejiang 310058, China

<sup>9</sup>Institute of Human Virology, Key Laboratory of Tropical Disease Control of Ministry of Education, Zhongshan School of Medicine, Sun Yat-sen University, Guangzhou, Guangdong 510080, China

<sup>10</sup>These authors contributed equally

<sup>11</sup>Lead contact

\*Correspondence: [dengkai6@mail.sysu.edu](mailto:dengkai6@mail.sysu.edu) (K.D.), [zchenai@hku.hk](mailto:zchenai@hku.hk) (Z.C.), [yelilincmv@tmmu.edu.cn](mailto:yelilincmv@tmmu.edu.cn) (L.Y.), [zhuyongqun@zju.edu.cn](mailto:zhuyongqun@zju.edu.cn) (Y.Z.)  
<https://doi.org/10.1016/j.chom.2022.03.035>

## SUMMARY

The SARS-CoV-2 Omicron variant harbors more than 30 mutations in the spike protein, leading to immune evasion from many therapeutic neutralizing antibodies. We reveal that a receptor-binding domain (RBD)-targeting monoclonal antibody, 35B5, exhibits potent neutralizing efficacy to Omicron. Cryo-electron microscopy structures of the extracellular domain trimer of Omicron spike with 35B5 Fab reveal that Omicron spike exhibits tight trimeric packing and high thermostability, as well as significant antigenic shifts and structural changes, within the RBD, N-terminal domain (NTD), and subdomains 1 and 2. However, these changes do not affect targeting of the invariant 35B5 epitope. 35B5 potently neutralizes SARS-CoV-2 Omicron and other variants by causing significant conformational changes within a conserved N-glycan switch that controls the transition of RBD from the “down” state to the “up” state, which allows recognition of the host entry receptor ACE2. This mode of action and potent neutralizing capacity of 35B5 indicate its potential therapeutic application for SARS-CoV-2.

## INTRODUCTION

The major concern of the COVID-19 pandemic is the emerging antigenic shifted SARS-CoV-2 variants of concern (VOCs) (Williams and Burgers, 2021; Yuan et al., 2021). Previously, SARS-CoV-2 VOCs, especially the Delta (B.1.617.2) variant identified in early 2021 (Cherian et al., 2021), harbored enhanced transmission and pathogenicity and showed resistance to a variety of therapeutic neutralizing antibodies, as well as COVID-19 vaccines (Corti et al., 2021). This concern is further amplified by a novel SARS-CoV-2 Omicron VOC (B.1.1.529), which was first described in South Africa in November 2021 and rapidly became dominant worldwide (He et al., 2021; Pulliam et al., 2021; Scott et al., 2021).

The Omicron variant is characterized by 37 spike (S) amino acid mutations, including 15 mutations in the RBD (Cameroni et al., 2021; Dejnirattisai et al., 2022; Hoffmann et al., 2022), the primary target for neutralizing antibodies. Very recent studies have indicated that the Omicron variant is markedly resistant to the majority of therapeutic neutralizing monoclonal antibodies (mAbs) approved for clinical use (Cameroni et al., 2021; Cao et al., 2022; Dejnirattisai et al., 2022; Hoffmann et al., 2022; Liu et al., 2021). Furthermore, the Omicron variant also escapes current COVID-19 vaccines (Cameroni et al., 2021; Hoffmann et al., 2022; Liu et al., 2021), including BNT162b2 (Pfizer) and mRNA-1273 (Moderna) (Baden et al., 2021; Polack et al., 2020; van Doremalen et al., 2020). Neutralizing antibodies with potent efficacy to the Omicron variant are urgently demanded.

RBD-targeting neutralizing antibodies are classified into four classes or six subgroups, each of which covers a specific epitope. Neutralization of SARS-CoV-2 by these antibodies is carried out through mechanisms including ACE2 competition, ACE2 molecular mimicry, and Fc-receptor-mediated neutralization (Barnes et al., 2020; Park et al., 2022). N-linked glycosylation has important roles in viral pathology, including mediating protein folding and stability and shaping viral tropism (Choi et al., 2021; Li et al., 2020; Watanabe et al., 2020). Glycosylation shields specific epitopes to facilitate viral immune evasion (Grant et al., 2020; Reis et al., 2021; Wintjens et al., 2020). Beyond the shield function, the glycans at N165 and N234 from the N-terminal domain (NTD) in SARS-CoV-2 act a molecular switch to control the conformational transition of the RBD from the “down” state to the “up” state, which is required for the receptor to bind to ACE2 (Casalino et al., 2020; Henderson et al., 2020). N165 and N234 are conserved in SARS-CoV-1 and MERS-CoV, highlighting the common mechanism of RBD conformational transition in S proteins. In this study, we found that despite the significantly structural changes in the Omicron S protein, 35B5, an RBD-targeting mAb cloned from the memory B cells of a convalescent COVID-19 patient, shows potent neutralizing activities against the SARS-CoV-2 Omicron variant and other VOCs via a distinctive glycan-displacement mechanism, which distinguishes 35B5 from the previously identified neutralizing mAbs against SARS-CoV-2.

## RESULTS

### 35B5 exhibits nanomolar neutralizing efficacy to the Omicron variant

We tested the neutralizing activity of 35B5, which shows broad neutralization to the SARS-CoV-2 wild-type (WT) and the Alpha, Beta, and Delta variants *in vitro* and *in vivo* (Wang et al., 2021), to the Omicron variant. 35B5 exhibited high binding capacity to the Omicron S protein ( $EC_{50} = 0.0618 \mu\text{g/mL}$ )—comparable to that to the WT ( $EC_{50} = 0.0195 \mu\text{g/mL}$ ) and Delta ( $EC_{50} = 0.0207 \mu\text{g/mL}$ ) S proteins (Figure 1A)—in enzyme-linked immunosorbent assays (ELISAs). *In vitro* incubation with 35B5 led to complete dissociation of the Omicron S trimer (Figure 1B). SARS-CoV-2-pseudovirus-based inhibition assays revealed that 35B5 exhibits potent neutralizing efficacy to the Omicron variant ( $IC_{50} = 0.0147 \mu\text{g/mL}$ ), as well as to SARS-CoV-2 WT ( $IC_{50} = 0.0024 \mu\text{g/mL}$ ) and the Delta variant ( $IC_{50} = 0.0069 \mu\text{g/mL}$ ) (Figure 1C). Echoing the pseudovirus-based inhibition assays, 35B5 potentially neutralizes infection with the authentic SARS-CoV-2 Omicron variant with an  $IC_{50}$  value of  $0.0499 \mu\text{g/mL}$  (Figure 1D). Thus, 35B5 harbors nanomolar neutralizing efficacy to the Omicron variant.

### Complex structure of Omicron spike-ECD trimer with 35B5 Fab

We employed the cryo-electron microscopy (EM) single-particle method to determine the complex structure of the Omicron S ectodomain (Omicron S-ECD) trimer with 35B5 Fab. 35B5 Fab and the Omicron S-ECD trimer were mixed and incubated at a stoichiometric ratio of 3:1 for 20 s and then flash frozen into liquid ethane for sample preparation. Two cryo-EM structures of the Omicron S-ECD-35B5 Fab complexes were

successfully determined at overall resolutions of 3.0 and 3.4 Å. The density map for the up-RBD-35B5 Fab region was obtained at a resolution of 3.35 Å by further local refinements (Figures S1 and S2A–S2F; Table S1). The Omicron S-ECD trimer in both of the two complexes contains two up-RBDs and one down-RBD (Figures 2A–2C). Each up-RBD is bound by a 35B5 Fab. One up-RBD domain in the S-ECD trimer of the complex at 3.0 Å resolution lacks clear densities, probably because 35B5 Fab causes conformational dynamics of the up-RBD.

Structural superposition of the Omicron and G614 S trimers via alignment by the S2 region revealed that the Omicron S-ECD trimer exhibits tighter structural packing. The NTD and RBD of Omicron notably move inward to the central S2 helical regions (Zhang et al., 2020) (Figure 2D). The mutation H655Y in the Omicron subdomain 2 (SD2) interacts with F643 and thereby increases the stability of the 630 loop (residues 617–644). The highly structured 630 loop further induces a more ordered structure of the fusion peptide proximal region (FPPR; residues 823–862) in the adjacent protomer to stabilize the down state of the RBD (Wang et al., 2021) (Figures 2E and 2F). The tighter trimeric packing and the more ordered FPPR suggest that the Omicron S trimer is more stable and resistant to premature dissociation. Consistently, differential scanning calorimetry assays revealed that the Omicron S-ECD trimer has higher thermostability than the G614 S-ECD protein (Figure S2G). The SARS-CoV-2 Omicron variant also exhibited higher environmental stability than the Alpha, Beta, and Delta variants on plastic and skin surfaces (Hirose et al., 2022).

### The RBD and NTD undergo significant antigenic shifts by Omicron mutations

The Omicron variant is characterized by 15 mutation sites in the RBD (Figure 3A). The 15 mutations induce significant structural changes of the mutant residues and antigenic shifts in the RBD. Most of the 15 mutation sites, including N501Y, G496S, K417N, Q493R, and G446S, are located in the loop regions of the ACE2-binding surface (Wang et al., 2020) (Figure 3A). These mutations severely change the epitopic residues of class 1 and 2 mAbs, such as C102, C002, and C121 (Barnes et al., 2020) (Figure S2H). The G339D and N440K mutations are located in the epitopes for class 3 mAbs, including C135 and S309, whereas S371L, S373P, and S375F are located at the RBD interface with class 4 mAbs, which generally harbor cross-species neutralizing activities to SARS-CoV and MERS-CoV (Figure S2H). Not only do the mutant residues contain structural changes, but the surface electrostatic distribution of the Omicron RBD is also notably altered; for example, there are increased positive charges in the class 1 and 2 mAb epitopes and an enhanced hydrophobic surface at the class 4 mAb interface (Figure 3B).

The NTD of the S protein is another important antigen for many neutralizing antibodies (Cerutti et al., 2021; Chi et al., 2020) and plays a role in the S stability through binding the RBD of the adjacent protomer (Shang et al., 2020). Compared with the WT NTD, the Omicron NTD has eight mutation sites, among which T95I and A67V increase the inner hydrophobic interactions in the central core region of the NTD (Figures S3A–S3C). The del69–70, del143–145, and ins214EPE mutations lead to the more

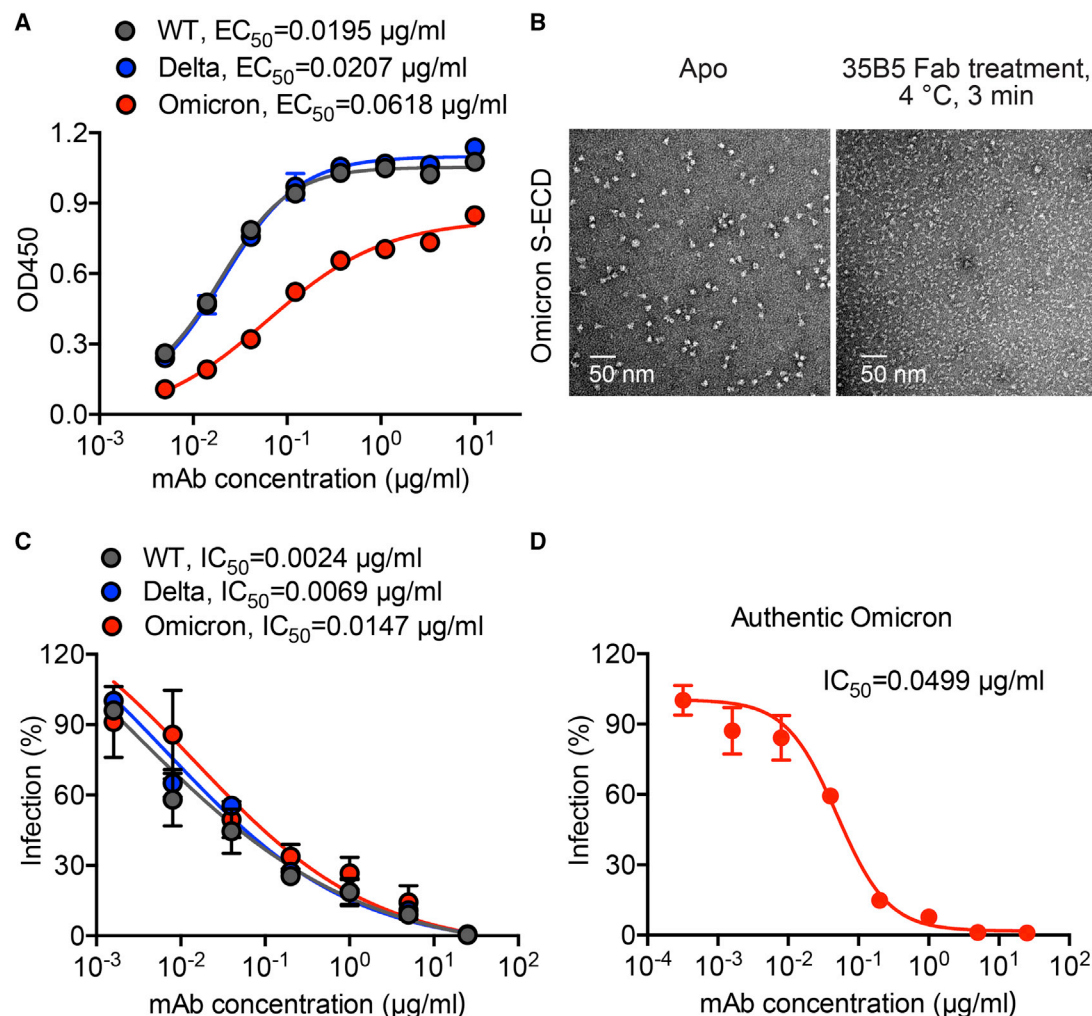


**Figure 1. Neutralizing activity of 35B5 against SARS-CoV-2 variants**

(A) Binding capacities and neutralizing activities of 35B5 against the S proteins of the SARS-CoV-2 WT and the Delta and Omicron variants. (B) Representative negative-staining EM micrographs of the Omicron S-ECD trimer after the treatment of 35B5. The Omicron S-ECD (the stable S-HexaPro mutant) trimer proteins were treated with or without 35B5 for 3 min at 4°C before negative-staining analysis. Scale bar, 50 nm. (C) Binding capacities and neutralizing activities of 35B5 against the pseudoviruses of the SARS-CoV-2 WT and the Delta and Omicron variants. (D) Neutralizing activity of 35B5 against the authentic SARS-CoV-2 Omicron. Data in (A), (C), and (D) are representative of one independent experiment out of two or three. Error bars in (A), (C), and (D) indicate the SEM.

disordered loop regions that are invisible in the density map (Figure S3A), whereas G142D and L212I are located on the surface, thereby generating antigenic shifts of the NTD and impairing the neutralizing activities of the mAbs that target the NTD (Figure S3A).

Omicron S2 contains six mutations in the central helical region (Figure 3C). In the structure of Omicron S-ECD, N764K and N856K generate two more hydrogen bonds and thus strengthen the interactions between S2 and the N2R linker (Gobeil et al., 2021) that connects the NTD and RBD and between S2 and subdomain 1 (SD1), respectively (Figures 3D and 3E). D796Y, L981F, and N969K increase the hydrophobic and hydrogen-bond interactions between the central helices in S2 (Figures S3D–S3F). The formation of more intra-trimer interactions results in the tighter packing of the Omicron S trimer.

### 35B5 targets the Omicron RBD via an invariant epitope

Despite the significant antigenic shifts and structural changes of Omicron S-ECD, 35B5 still binds to the Omicron RBD at an interface covering an area of  $1,006 \text{ \AA}^2$  (Figures 3F and S3G) via the heavy-chain complementarity-determining regions CDRH2 and CDRH3 and the heavy-chain framework FRH3 (Figures 3F and S3G). The epitope in the Omicron RBD for 35B5 is composed of 29 interacting residues, including R346, F347, N354, R466, A352, K444, Y449, N450, R466, I468, T470, and F490 (Figures 3F and S3G). At the interface, hydrogen bonds and salt bridges generate an interaction network and play central roles in the interactions. Specifically, T345<sup>RBD</sup> forms a hydrogen bond with D112<sup>35B5</sup>, and R346<sup>RBD</sup> forms a salt bridge with E114<sup>35B5</sup>. G66<sup>35B5</sup> interacts with Y449<sup>RBD</sup> through a main-side chain hydrogen bond, whereas R466, Y351, and

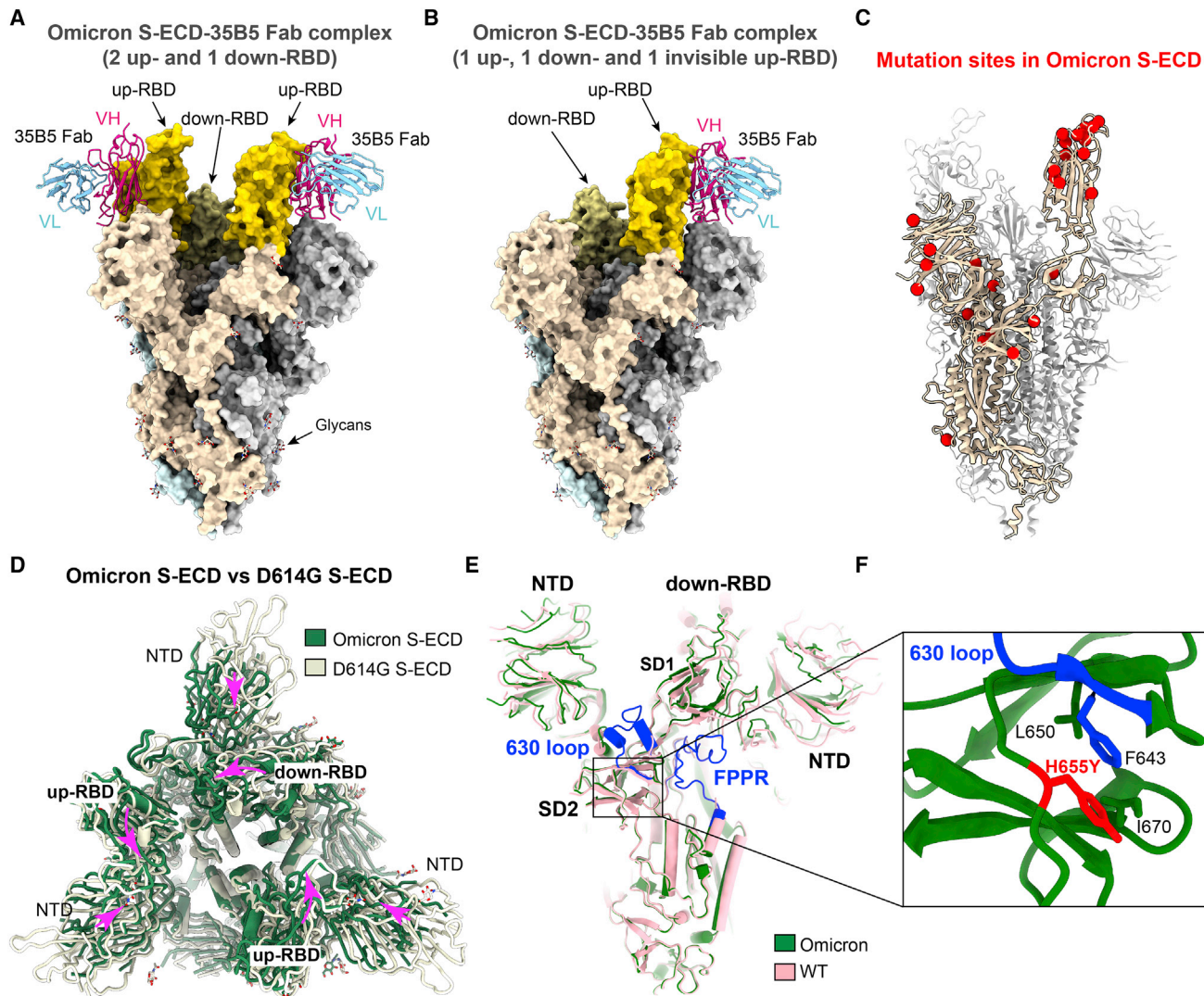


**Figure 2. Cryo-EM structure of the Omicron S-ECD complexed with 35B5 Fab**

(A and B) Cryo-EM structures of the Omicron S-ECD trimer complexed with 35B5 Fab at resolutions of 3.4 Å (A) and 3.0 Å (B). The Omicron S trimer is shown as a surface. The VH and VL domains of 35B5 Fab are shown as cartoons and colored in pink and cyan, respectively. The up- and down-RBDs are highlighted in yellow and light yellow, respectively.

(C) Mutation sites (highlighted as red spheres) in the Omicron S promoter.

(D) Structural comparison of the Omicron S-ECD with the G614 S-ECD (PDB: 7BNO). The S-ECD trimers of Omicron and G614 are colored in green and gray, respectively. The NTD and RBD are labeled as indicated. Conformational changes are indicated with purple arrows.

(E) Structural comparison of the closed promoters from the Omicron (green) and WT (light pink; PDB: 7E9N) S trimers. The ordered 630 loop and adjacent FPPRs are highlighted in red. SD1, SD2, the down-RBD, and the NTD are labeled as indicated.

(F) Enlarged view of the interactions between H655Y and the Omicron 630 loop.

T470 are contacted by S55<sup>35B5</sup>, S71<sup>35B5</sup>, and H82<sup>35B5</sup> via side-chain-mediated hydrogen bonds (Figures S3H and S3I). In addition to hydrogen bonds and salt bridges, hydrophobic interactions largely participate in the 35B5-Omicron RBD interactions and stabilize the 35B5-RBD interface (Figures S3H and S3I). However, the hydrogen bond between R16<sup>35B5</sup> and N481<sup>RBD</sup> in the previously determined WT RBD-35B5 Fab structure (Wang et al., 2021) is impaired at the Omicron RBD-35B5 Fab interface, which is the likely cause of the slightly weaker binding affinity of 35B5 to the Omicron S trimer than to the WT S trimer.

Further sequence analysis revealed that the epitopic residues for 35B5 in the RBD are invariant in SARS-CoV-2 WT and the Alpha, Beta, Delta, Lambda, and Omicron variants (Figure S4A). Among the 15 mutation sites in the Omicron RBD, G339D, G446S, and E484A are located at the edge of the 35B5-RBD interface (Figure 3G) but have no structural collision with 35B5 Fab (Figure 3G). The other 12 mutations are located far from the epitope for 35B5 (Figure 3G). Thus, the invariant epitopic residues for 35B5 provide the molecular basis for efficient targeting of the Omicron RBD by 35B5. In addition, the Omicron S trimer maintains the down-RBD-NTD interface as the same as that in

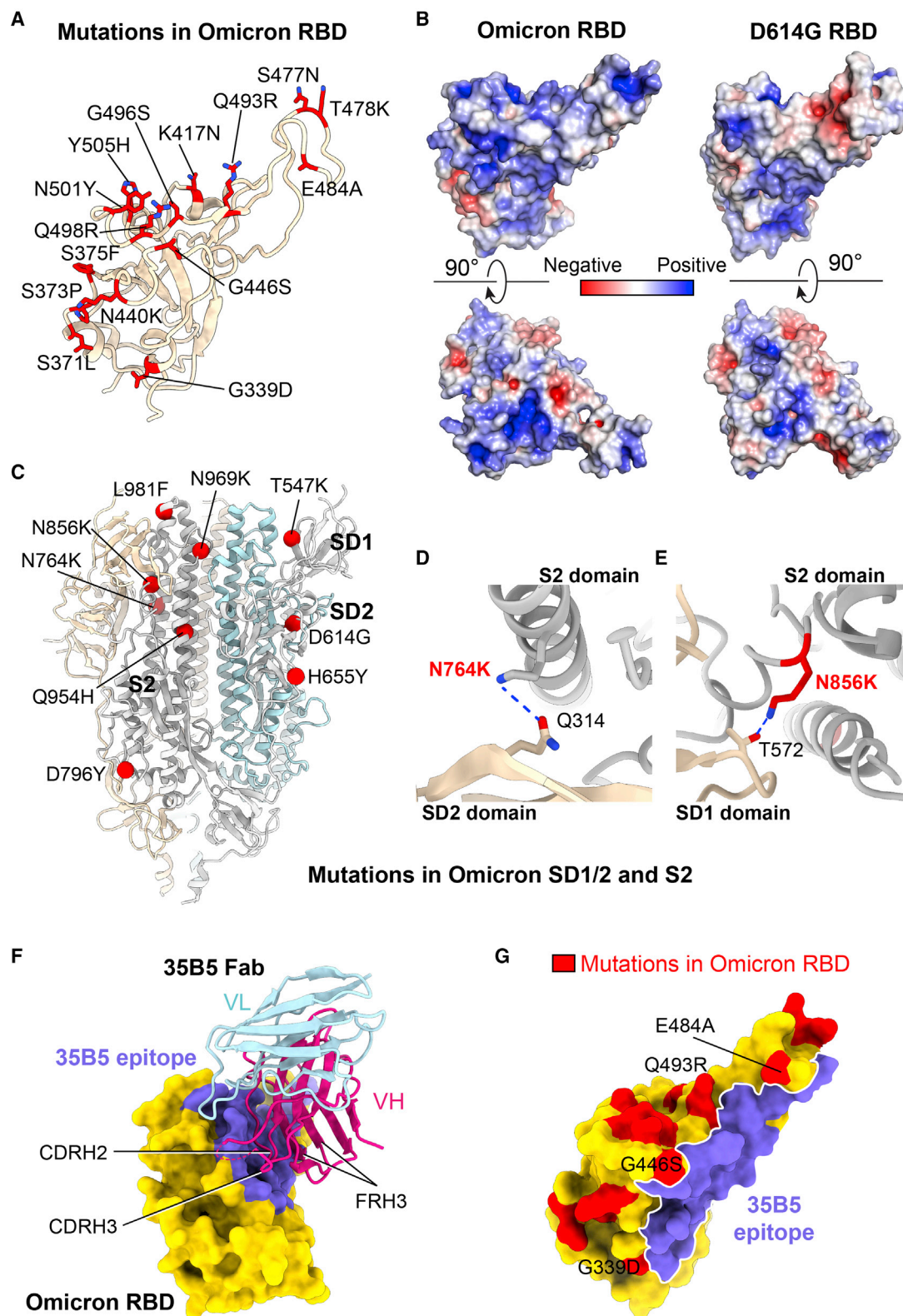


**Figure 3. Mutation effects on the structure of the Omicron S protein**

(A) Mutation sites in the Omicron RBD. The mutation residues are shown as red sticks.

(B) Surface electrostatic distribution of Omicron (left) and G614 (right) RBDs colored by relative electrostatic potential (red, negatively charged; blue, positively charged).

(legend continued on next page)

the other variants. Correspondingly, the epitopic residues E340, T345, R346, K444, Y449, and N450 for 35B5 are solvent exposed in the Omicron down-RBD, which allows initial recognition by 35B5 (Figures S4B and S4C).

### The L2 loop in the 35B5 epitope is essential for RBD structural integrity and ACE2 binding

We then investigated the roles of the 35B5 invariant epitope in the S structure. The ACE2-binding surface on the RBD (Figures 4A and 4I) is constituted by the  $\beta 5$ - $\beta 6$  antiparallel sheet with linking loops and  $\alpha$  helices, suggesting that the stability of the  $\beta 5$ - $\beta 6$  sheet determines ACE2 binding during SARS-CoV-2 infection. In the RBD structure, the 35B5 epitopic residues R346, S349, and Y351 are located in the L2 loop (residues 344–354) and interact with Y451 in  $\beta 5$ , L452 in  $\beta 5$ , and L492 in  $\beta 6$ , respectively, to stabilize the conformations of the two  $\beta$  strands (Figure 4A). Moreover, residue V350 at the turn in the L2 loop inserts into the hydrophobic pocket under  $\beta 5$ , which provides a firm basis to support the strand (Figure 4A). These extensive interactions suggest that L2 and its containing 35B5 epitopic residues are crucial for the stability maintenance of  $\beta 5$  and  $\beta 6$  and thereby determine ACE2 binding during viral invasion (Wang et al., 2020).

### The epitopic residues of 35B5 control the conformational dynamics of the RBD

The RBD transits from the down state to the up state required for ACE2 recognition. The N-glycans at residues N165 and N234 in the NTD clamp the two sides of the RBD and function as a switch to control the conformational transition (Casalino et al., 2020; Henderson et al., 2020) (Figure 4B). The N165A mutation causing glycan deletion at N165 results in a discernable increase in up-state RBDs, and the N165Q mutant of the S trimer is more sensitive to RBD-targeting mAbs, highlighting the key role of the N165-glycans in maintaining the closed conformation of the down-RBD (Henderson et al., 2020; Li et al., 2020). In the S trimer, the N165-glycans extend toward the down-RBD and are bound into the shallow pocket in the 35B5 epitope (Figure 4C). The conserved epitopic residues Y351, T470, F490, and L452 make extensive interactions with the glycans, suggesting that these residues are crucial for the function of the N165-glycan (Figures 4C and 4D). In addition, the 35B5-interacting residues R466 and I468 bind to the NTD below the down-RBD interface with the N165-glycans (Figure 4D). Thus, the 35B5 epitopic residues control the conformational dynamics of the RBD by binding the N165-glycans from the NTD.

### 35B5 binding causes significant conformational changes of the glycan switch

Superimposition of the 35B5-bound RBD and NTD with the down-RBD with its bound adjacent NTD in the Omicron S-ECD-35B5 Fab complex revealed that upon 35B5 Fab binding, the N165-glycans are displaced from their binding shallow

pocket in the up-RBD (Figures 4B, 4E, and 4G). The N234-glycans are also completely released into the solvent, whereas the N234-glycans have direct contacts with the up-RBD in the WT and G614 S trimers (Figures 4E, 4F and 4H). Displacement of the N165-glycans was also observed in the initial recognition of the exposed epitopic residues of the down-RBD by 35B5, which was captured in our previously determined state I structure of the WT S-ECD-35B5 Fab complex (Wang et al., 2021) (Figure S4D). The displacement and dysfunction of the glycan switch at N165 and N234 of the NTD by 35B5 most likely lead to the unstable up states of the RBD (Wrapp et al., 2020) and finally cause the dissociation of the S trimer (Wang et al., 2021).

## DISCUSSION

The Omicron S protein harbors significant antigenic shifts and structural changes, leading to immune escape of the Omicron variant from most mAbs. Our previous study had shown that 35B5 has neutralizing activities against the WT and the Beta and Delta variants of SARS-CoV-2. 35B5 dissociates the S trimer and neutralizes SARS-CoV-2 through four steps via an epitope that avoids the prevailing mutation sites on the RBD in the Beta and Delta variants. In this study, we found that 35B5 could neutralize the Omicron variant with a potent neutralizing efficacy much higher than that of many other neutralizing antibodies. The actual reason why the S protein dissociates is that 35B5 displaces the conserved glycan switch from the RBD, leading to the unstable up states of the RBD and eventually causing the shedding of S1 from the S trimer. The invariant epitope in the RBD for 35B5 is distinct from those of the previously identified four classes of RBD-targeting mAbs. The glycan-displacement action of 35B5 represents an unprecedented neutralizing action of mAbs against SARS-CoV-2, which is different from the previously determined ACE2 competition and molecular mimicry mechanisms utilized by class 1 and 2 RBD mAbs and the Fc-receptor-mediated neutralizing mechanisms of class 3 and 4 RBD mAbs (Barnes et al., 2020; Park et al., 2022).

The 35B5 epitope contains a few residues of the epitopes of the class 3 mAbs (Barnes et al., 2020). These overlapping invariant epitopic residues are far from the mutation sites in the Omicron RBD. Further screening and re-examination of the neutralizing activities of the class 3 mAb against the Omicron variant will be valuable. In addition, it is also possible that a few class 1 mAbs are tolerant of the antigenic shifts of Omicron as a result of mutation-enhanced binding affinity and invariant interacting residues (Cameroni et al., 2021).

The Omicron S trimer has a tight structure and is stable and resistant to premature dissociation. Despite the structural changes and significant antigenic shifts caused by the 37 mutations in Omicron S, the epitope for 35B5 remains invariant in Omicron and other VOCs during viral evolution. The 35B5 epitopic residues are essential for RBD structural integrity and

(C) Mutation sites in Omicron SD1 and SD2 and the S2 region. The mutant residues are illustrated as red balls and labeled as indicated.

(D and E) The effects of N764K (D) and N856K (E) on the S2-SD2 interactions. Potential hydrogen bonds are highlighted as blue dashed lines.

(F) Interactions between 35B5 Fab and the Omicron RBD (shown as a yellow surface). The epitope for 35B5 Fab is highlighted in blue. The VH and VL domains are shown as cartoons and colored in red and cyan, respectively. The interacting regions FRH3, CDRH2, and CDRH3 of 35B5 are labeled as indicated.

(G) Surface distributions of the Omicron mutation sites and the epitope for 35B5 on the RBD (colored in yellow). The 35B5 epitope and Omicron mutations are highlighted in blue and red, respectively.

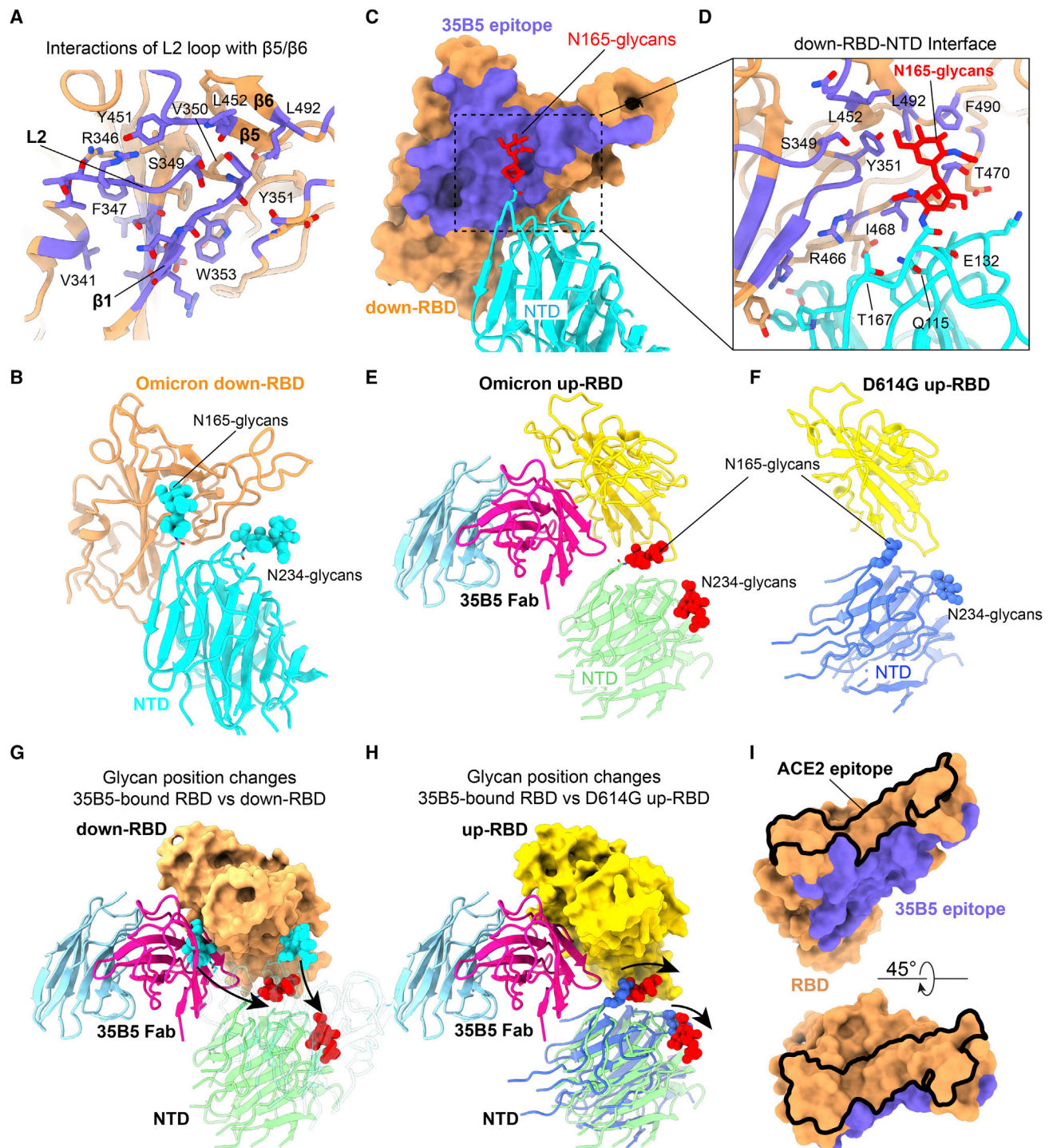


**Figure 4. Glycan displacement by 35B5 from the RBD**

(A) Interactions between the L2 loop and  $\beta 5$  and  $\beta 6$  in the core region of the Omicron RBD.

(B) Location of the N165- and N234-glycans from the NTD at the interface between the NTD and the down-RBD in Omicron S-ECD. The N165- and N234-glycans are colored in red and light blue, respectively. The glycans are shown as spheres.

(C) Interface between the N165-glycans and the down-RBD in Omicron S-ECD. The down-RBD and N165-glycans are shown as a surface and sticks, respectively.

(D) Detailed interactions between the down-RBD and the N165-glycans. The interacting residues are shown as sticks and labeled as indicated.

(E and F) Interactions between the N165- and N234-glycans and the up-RBDs in the Omicron S-ECD-35B5 Fab complex (E) and the G614 S-ECD trimer (F).

(legend continued on next page)

conformational dynamics, which are required for ACE2 binding and S stability (Figures 4A and 4I). These structural characteristics provide the molecular basis of the potent neutralization and high antigenic-shift tolerance of 35B5 against the Omicron variant. The invariant epitope for 35B5 indicates that it will retain potent neutralizing activity against new SARS-CoV-2 variants that might emerge in the future. The potent neutralizing efficacy and high antigenic-shift tolerance of 35B5 make it a good candidate in clinical therapy and indicate the potential application of its specific epitope in a universal vaccine against SARS-CoV-2 VOCs.

## STAR★METHODS

Detailed methods are provided in the online version of this paper and include the following:

- **KEY RESOURCES TABLE**
- **RESOURCE AVAILABILITY**
  - Lead contact
  - Materials availability
  - Data and code availability
- **EXPERIMENTAL MODEL AND SUBJECT DETAILS**
  - Cell lines
  - Virus strains
- **METHOD DETAILS**
  - Monoclonal antibody
  - ELISA
  - SARS-CoV-2 pseudovirus neutralization
  - Authentic SARS-CoV-2 Omicron neutralization
  - Production and purification of Omicron S-ECD and 35B5 Fab proteins
  - Differential scanning fluorimetry
  - Negative-staining analysis
  - Cryo-EM sample preparation and data collection
  - Cryo-EM image processing
  - Cryo-EM structure modeling and analysis
- **QUANTIFICATION AND STATISTICAL ANALYSIS**

## SUPPLEMENTAL INFORMATION

Supplemental information can be found online at <https://doi.org/10.1016/j.chom.2022.03.035>.

## ACKNOWLEDGMENTS

We thank the core facility of the Life Sciences Institute for negative-staining imaging and the facility members of the Cryo-EM Center of Zhejiang University for assistance in cryo-EM data collection. This work was supported by grants from the National Natural Science Foundation of China (81925024 to Y. Zhu, 31825011 to L.Y., and 82002103 to X.W.), the National Science and Technology Major Project of the Ministry of Science and Technology of China (2017ZX10202102-006-002 to L.Y. and 2017YFA0503900 to Y. Zhu), the Guangdong Innovative and Entrepreneurial Research Team Program (2016ZT06S638 to K.D.), the National High-Level Talents Special Support Program (to Y. Zhou), and the Fundamental Research Funds for the Central Universities (to Y. Zhu).

## AUTHOR CONTRIBUTIONS

X.W., J.T., and Y.X. performed negative-staining and cryo-EM analyses; X.C., S.Y., Y.L., and Y.Y. cloned and produced the 35B5 mAb and performed SARS-CoV-2-pseudovirus-based neutralization assays; R.Z. performed authentic SARS-CoV-2-Omicron-based neutralization assays; Z.C., K.D., and Y.Z. prepared the reagents; Y. Zhu and L.Y. designed the study, analyzed the data, and wrote the paper with X.C., X.W., and J.T.; and Y. Zhu and L.Y. supervised the study.

## DECLARATION OF INTERESTS

The patent of 35B5 has been licensed. K.D. and Y. Zhu are listed as inventors of the patent.

Received: January 31, 2022

Revised: March 9, 2022

Accepted: March 25, 2022

Published: March 28, 2022

## REFERENCES

- Adams, P.D., Afonine, P.V., Bunkoczi, G., Chen, V.B., Davis, I.W., Echols, N., Headd, J.J., Hung, L.W., Kapral, G.J., Grosse-Kunstleve, R.W., et al. (2010). PHENIX: a comprehensive Python-based system for macromolecular structure solution. *Acta Crystallogr. D Biol. Crystallogr.* 66, 213–221. <https://doi.org/10.1107/s0907444909052925>.
- Baden, L.R., El Sahly, H.M., Essink, B., Kotloff, K., Frey, S., Novak, R., Diemert, D., Spector, S.A., Rouphael, N., Creech, C.B., et al. (2021). Efficacy and safety of the mRNA-1273 SARS-CoV-2 vaccine. *N. Engl. J. Med.* 384, 403–416. <https://doi.org/10.1056/nejmoa2035389>.
- Barnes, C.O., Jette, C.A., Abernathy, M.E., Dam, K.M.A., Esswein, S.R., Gristick, H.B., Malyutin, A.G., Sharaf, N.G., Huey-Tubman, K.E., Lee, Y.E., et al. (2020). SARS-CoV-2 neutralizing antibody structures inform therapeutic strategies. *Nature* 588, 682–687. <https://doi.org/10.1038/s41586-020-2852-1>.
- Cameron, E., Saliba, C., Bowen, J.E., Rosen, L.E., Culap, K., Pinto, D., De Marco, A., Kaiser, H., Noack, J., Farhat, N., et al. (2021). Broadly neutralizing antibodies overcome SARS-CoV-2 Omicron antigenic shift. Preprint at bioRxiv. <https://doi.org/10.1101/2021.12.12.472269>.
- Cao, Y., Wang, J., Jian, F., Xiao, T., Song, W., Yisimayi, A., Huang, W., Li, Q., Wang, P., An, R., et al. (2022). Omicron escapes the majority of existing SARS-CoV-2 neutralizing antibodies. *Nature* 602, 657–663. <https://doi.org/10.1038/s41586-021-04385-3>.
- Casalino, L., Gaieb, Z., Goldsmith, J.A., Hjorth, C.K., Dommer, A.C., Harbison, A.M., Fogarty, C.A., Barros, E.P., Taylor, B.C., McLellan, J.S., et al. (2020). Beyond shielding: The roles of glycans in the SARS-CoV-2 spike protein. *ACS Cent. Sci.* 6, 1722–1734. <https://doi.org/10.1021/acscentsci.0c01056>.
- Cerutti, G., Guo, Y., Zhou, T., Gorman, J., Lee, M., Rapp, M., Reddem, E.R., Yu, J., Bahna, F., Bimela, J., et al. (2021). Potent SARS-CoV-2 neutralizing antibodies directed against spike N-terminal domain target a single supersite. *Cell Host Microbe* 29, 819–833.e7. <https://doi.org/10.1016/j.chom.2021.03.005>.
- Cherian, S., Potdar, V., Jadhav, S., Yadav, P., Gupta, N., Das, M., Rakshit, P., Singh, S., Abraham, P., and Panda, S.; NIC Team (2021). SARS-CoV-2 spike mutations, L452R, T478K, E484Q and P681R, in the second wave of COVID-19 in Maharashtra, India. *Microorganisms* 9, 1542. <https://doi.org/10.3390/microorganisms9071542>.
- Chi, X., Yan, R., Zhang, J., Zhang, G., Zhang, Y., Hao, M., Zhang, Z., Fan, P., Dong, Y., Yang, Y., et al. (2020). A neutralizing human antibody binds to the

(G and H) Glycan position changes upon 35B5 binding. The 35B5-bound RBD and NTD (E) were superimposed with the down-RBD with its bound NTD (B) to illustrate the glycan displacement by 35B5 from the down-RBD (G). The 35B5-bound RBD and NTD (E) were superimposed with the D614G up-RBD with its bound NTD (F) to illustrate the glycan position changes in the two structures (H). Glycan position changes induced by 35B5 are indicated by black arrows.

(I) The ACE2 epitope, (contoured with a black outline) is compared with the 35B5 epitope (colored in blue). The ACE2-bound RBD from the structure of Omicron S-ECD complexed with ACE2 (PDB: 7T9L) is illustrated for the epitope for ACE2.

N-terminal domain of the Spike protein of SARS-CoV-2. *Science* 369, 650–655. <https://doi.org/10.1126/science.abc6952>.

Choi, Y.K., Cao, Y., Frank, M., Woo, H., Park, S.J., Yeom, M.S., Croll, T.I., Seok, C., and Im, W. (2021). Structure, dynamics, receptor binding, and antibody binding of the fully glycosylated full-length SARS-CoV-2 spike protein in a viral membrane. *J. Chem. Theor. Comput* 17, 2479–2487. <https://doi.org/10.1021/acs.jctc.0c01144>.

Corti, D., Purcell, L.A., Snell, G., and Veesler, D. (2021). Tackling COVID-19 with neutralizing monoclonal antibodies. *Cell* 184, 3086–3108. <https://doi.org/10.1016/j.cell.2021.05.005>.

Dejnirattisai, W., Huo, J., Zhou, D., Zahradník, J., Supasa, P., Liu, C., Duyvesteyn, H.M.E., Ginn, H.M., Mentzer, A.J., Tuekprakhon, A., et al. (2022). SARS-CoV-2 Omicron-B. 1.1. 529 leads to widespread escape from neutralizing antibody responses. *Cell* 185, 467–484.e15. <https://doi.org/10.1016/j.cell.2021.12.046>.

Emsley, P., Lohkamp, B., Scott, W.G., and Cowtan, K. (2010). Features and development of Coot. *Acta Crystallogr. D Biol. Crystallogr.* 66, 486–501. <https://doi.org/10.1107/s0907444910007493>.

Gobeil, S.M.C., Janowska, K., McDowell, S., Mansouri, K., Parks, R., Manne, K., Stalls, V., Kopp, M.F., Henderson, R., Edwards, R.J., et al. (2021). D614G mutation alters SARS-CoV-2 spike conformation and enhances protease cleavage at the S1/S2 junction. *Cell Rep.* 34, 108630. <https://doi.org/10.1016/j.celrep.2020.108630>.

Goddard, T.D., Huang, C.C., Meng, E.C., Pettersen, E.F., Couch, G.S., Morris, J.H., and Ferrin, T.E. (2018). UCSF ChimeraX: Meeting modern challenges in visualization and analysis. *Protein Sci.* 27, 14–25. <https://doi.org/10.1002/pro.3235>.

Grant, O.C., Montgomery, D., Ito, K., and Woods, R.J. (2020). Analysis of the SARS-CoV-2 spike protein glycan shield reveals implications for immune recognition. *Sci. Rep.* 10, 14991. <https://doi.org/10.1038/s41598-020-71748-7>.

He, X., Hong, W., Pan, X., Lu, G., and Wei, X. (2021). SARS-CoV-2 Omicron variant: Characteristics and prevention. *MedComm* 2, 838–845. <https://doi.org/10.1002/mco2.110>.

Henderson, R., Edwards, R.J., Mansouri, K., Janowska, K., Stalls, V., Kopp, M., Haynes, B.F., and Acharya, P. (2020). Glycans on the SARS-CoV-2 spike control the receptor binding domain conformation. Preprint at bioRxiv. <https://doi.org/10.1101/2020.06.26.173765>.

Hirose, R., Itoh, Y., Ikegaya, H., Miyazaki, H., Watanabe, N., Yoshida, T., Bandou, R., Daidoji, T., and Nakaya, T. (2022). Differences in environmental stability among SARS-CoV-2 variants of concern: Omicron has higher stability. Preprint at bioRxiv. <https://doi.org/10.1101/2022.01.18.476607>.

Hoffmann, M., Krüger, N., Schulz, S., Cossmann, A., Rocha, C., Kempf, A., Nehlmeier, I., Graichen, L., Moldenhauer, A.-S., Winkler, M.S., et al. (2022). The Omicron variant is highly resistant against antibody-mediated neutralization—implications for control of the COVID-19 pandemic. *Cell* 185, 447–456.e11. <https://doi.org/10.1016/j.cell.2021.12.032>.

Li, Q., Wu, J., Nie, J., Zhang, L., Hao, H., Liu, S., Zhao, C., Zhang, Q., Liu, H., Nie, L., et al. (2020). The impact of mutations in SARS-CoV-2 spike on viral infectivity and antigenicity. *Cell* 182, 1284–1294.e9. <https://doi.org/10.1016/j.cell.2020.07.012>.

Liu, L., Iketani, S., Guo, Y., Chan, J.F.-W., Wang, M., Liu, L., Luo, Y., Chu, H., Huang, Y., and Nair, M.S. (2021). Striking antibody evasion manifested by the Omicron variant of SARS-CoV-2. Preprint at bioRxiv. <https://doi.org/10.1101/2021.12.14.472719>.

Mastroratte, D.N. (2005). Automated electron microscope tomography using robust prediction of specimen movements. *J. Struct. Biol.* 152, 36–51. <https://doi.org/10.1016/j.jsb.2005.07.007>.

Park, Y.J., De Marco, A., Starr, T.N., Liu, Z., Pinto, D., Walls, A.C., Zatta, F., Zepeda, S.K., Bowen, J.E., Sprouse, K.R., et al. (2022). Antibody-mediated broad sarbecovirus neutralization through ACE2 molecular mimicry. *Science* 375, 449–454. <https://doi.org/10.1126/science.abm8143>.

Polack, F.P., Thomas, S.J., Kitchin, N., Absalon, J., Gurtman, A., Lockhart, S., Perez, J.L., Perez Marc, G., Moreira, E.D., Zerbini, C., et al. (2020). Safety and

efficacy of the BNT162b2 mRNA covid-19 vaccine. *N. Engl. J. Med.* 383, 2603–2615. <https://doi.org/10.1056/nejmoa2034577>.

Pulliam, J.R., van Schalkwyk, C., Govender, N., von Gottberg, A., Cohen, C., Groome, M.J., Dushoff, J., Mlisana, K., and Moultrie, H. (2021). Increased risk of SARS-CoV-2 reinfection associated with emergence of the Omicron variant in South Africa. Preprint at medRxiv. <https://doi.org/10.1101/2021.11.11.21266068>.

Punjani, A., Rubinstein, J.L., Fleet, D.J., and Brubaker, M.A. (2017). cryoSPARC: Algorithms for rapid unsupervised cryo-EM structure determination. *Nat. Methods* 14, 290–296. <https://doi.org/10.1038/nmeth.4169>.

Reis, C.A., Tauber, R., and Blanchard, V. (2021). Glycosylation is a key in SARS-CoV-2 infection. *J. Mol. Med. (Berl)* 99, 1023–1031. <https://doi.org/10.1007/s00109-021-02092-0>.

Scott, L., Hsiao, N.Y., Moyo, S., Singh, L., Tegally, H., Dor, G., Maes, P., Pybus, O.G., Kraemer, M.U.G., Semenova, E., et al. (2021). Track Omicron's spread with molecular data. *Science* 374, 1454–1455. <https://doi.org/10.1126/science.abn4543>.

Shang, J., Ye, G., Shi, K., Wan, Y., Luo, C., Aihara, H., Geng, Q., Auerbach, A., and Li, F. (2020). Structural basis of receptor recognition by SARS-CoV-2. *Nature* 581, 221–224. <https://doi.org/10.1038/s41586-020-2179-y>.

van Doremalen, N., Lambe, T., Spencer, A., Belij-Rammerstorfer, S., Purushotham, J.N., Port, J.R., Avanzato, V.A., Bushmaker, T., Flaxman, A., Ulaszewska, M., et al. (2020). ChAdOx1 nCoV-19 vaccine prevents SARS-CoV-2 pneumonia in rhesus macaques. *Nature* 586, 578–582. <https://doi.org/10.1038/s41586-020-2608-y>.

Wang, Q., Zhang, Y., Wu, L., Niu, S., Song, C., Zhang, Z., Lu, G., Qiao, C., Hu, Y., Yuen, K.Y., et al. (2020). Structural and functional basis of SARS-CoV-2 entry by using human ACE2. *Cell* 181, 894–904.e9. <https://doi.org/10.1016/j.cell.2020.03.045>.

Wang, X., Hu, A., Chen, X., Zhang, Y., Yu, F., Yue, S., Li, A., Zhang, J., Pan, Z., Yang, Y., et al. (2021). A potent human monoclonal antibody with pan-neutralizing activities directly dislocates S trimer of SARS-CoV-2 through binding both up and down forms of RBD. Preprint at bioRxiv. <https://doi.org/10.1101/2021.11.29.470356>.

Watanabe, Y., Allen, J.D., Wrapp, D., McLellan, J.S., and Crispin, M. (2020). Site-specific glycan analysis of the SARS-CoV-2 spike. *Science* 369, 330–333. <https://doi.org/10.1126/science.abb9983>.

Williams, T.C., and Burgers, W.A. (2021). SARS-CoV-2 evolution and vaccines: Cause for concern? *Lancet Respir. Med.* 9, 333–335. [https://doi.org/10.1016/s2213-2600\(21\)00075-8](https://doi.org/10.1016/s2213-2600(21)00075-8).

Wintjens, R., Bifani, A.M., and Bifani, P. (2020). Impact of glycan cloud on the B-cell epitope prediction of SARS-CoV-2 spike protein. *NPJ Vaccin.* 5, 81. <https://doi.org/10.1038/s41541-020-00237-9>.

Wrapp, D., Wang, N., Corbett, K.S., Goldsmith, J.A., Hsieh, C.L., Abiona, O., Graham, B.S., and McLellan, J.S. (2020). Cryo-EM structure of the 2019-nCoV spike in the prefusion conformation. *Science* 367, 1260–1263. <https://doi.org/10.1126/science.abb2507>.

Yuan, M., Huang, D., Lee, C.C.D., Wu, N.C., Jackson, A.M., Zhu, X., Liu, H., Peng, L., van Gils, M.J., Sanders, R.W., et al. (2021). Structural and functional ramifications of antigenic drift in recent SARS-CoV-2 variants. *Science* 373, 818–823. <https://doi.org/10.1126/science.abh1139>.

Zhang, J., Cai, Y., Xiao, T., Lu, J., Peng, H., Sterling, S.M., Walsh, R.M., Rits-Volloch, S., Sliz, P., and Chen, B. (2020). Structural impact on SARS-CoV-2 spike protein by D614G substitution. Preprint at bioRxiv. <https://doi.org/10.1101/2020.10.13.337980>.

Zheng, S.Q., Palovcak, E., Armache, J.P., Verba, K.A., Cheng, Y., and Agard, D.A. (2017). MotionCorr2: Anisotropic correction of beam-induced motion for improved cryo-electron microscopy. *Nat. Methods* 14, 331–332. <https://doi.org/10.1038/nmeth.4193>.

Zhou, D., Xu, H., Poon, V.K.M., Yuan, S., Li, C., Chik, K.K.H., Cao, J., Kwan, K.Y., Du, Z., Lau, T.T.K., et al. (2021). Robust SARS-CoV-2 infection in nasal turbinates after treatment with systemic neutralizing antibodies. *Cell Host Microbe* 29, 551–563.e5. <https://doi.org/10.1016/j.chom.2021.02.019>.

## STAR★METHODS

### KEY RESOURCES TABLE

REAGENT or RESOURCE	SOURCE	IDENTIFIER
<b>Antibodies</b>		
35B5	this paper	N/A
HRP-conjugated anti-human IgG antibody	Bioss Biotech	Cat# bs-0297G-HRP; RRID: AB_10894725
ExpiCHO Expression System Kit	Thermo Fisher Scientific	Cat# A29133
TMB	Beyotime	Cat# P0209
Dual-Luciferase Reporter Assay System Kit	Promega	Cat# E1910
<b>Bacterial and virus strains</b>		
SARS-CoV-2 WT pseudovirus	Sino Biological	Cat# PSV001
SARS-CoV-2 Delta pseudovirus	Sino Biological	Cat# PSV011
SARS-CoV-2 Omicron pseudovirus	Sino Biological	Cat# PSV016
Authentic SARS-CoV-2 virus (HKU691)	this paper	N/A
<b>Chemicals, peptides, and recombinant proteins</b>		
Polyethylenimine	Polysciences	Cat# 24765-1
SMM 293-T1 medium	Sino Biological	Cat# M293T1
Papain	Worthington Biochemical Corporation	Cat# LS003119
SARS-CoV-2 WT S trimer protein	Acro Biosystems	Cat# SPN-C52H7
SARS-CoV-2 Delta S protein	Sino Biological	Cat# 40589-V08H10
SARS-CoV-2 Omicron S protein	Acro Biosystems	Cat# SPN-C52Hz
SARS-CoV-2 S protein (D614G), His Tag, HexaPro trimer	Acro Biosystems	Cat# SPN-C52H3
<b>Deposited data</b>		
Coordinates and cryo-EM map of the Omicron S-ECD-35B5 Fab (1 down- and 2 up-RBDs)	this paper	PDB: 7WLY; EMDB: EMD-32594
Coordinates and cryo-EM map of the Omicron S-ECD-35B5 Fab (1 up-, 1 down-, and 1 invisible up-RBD)	this paper	PDB: 7WLZ; EMDB: EMD-32595
Coordinates and cryo-EM map of the Omicron RBD-35B5 Fab (local refinement)	this paper	PDB: 7WM0; EMDB: EMD-32596
<b>Experimental models: Cell lines</b>		
HEK293F cells	Thermo Fisher Scientific	Cat# 11625019
HEK293T/ACE2 cells	this paper	N/A
<b>Recombinant DNA</b>		
SARS-CoV-2 S (Omicron variant) gene, residues 1–1208, 6P and furin cleavage mutation, T4 fibrin trimerization motif, 8xHisTag, pcDNA	this paper	N/A
5′-CGCATACAGTCTTRCAGGCT-3′	this paper	N/A
5′-GTGTGATGTTGAWATGACATGGTC-3′	this paper	N/A
<b>Software and algorithms</b>		
SerialEM	<a href="#">Mastrorade (2005)</a>	<a href="https://bio3d.colorado.edu/SerialEM/">https://bio3d.colorado.edu/SerialEM/</a>
MotionCor2	<a href="#">Zheng et al. (2017)</a>	<a href="https://msg.ucsf.edu/">https://msg.ucsf.edu/</a>
cryoSPARC	<a href="#">Punjani et al. (2017)</a>	<a href="https://cryosparc.com/">https://cryosparc.com/</a>
UCSF ChimeraX	<a href="#">Goddard et al. (2018)</a>	<a href="https://www.cgl.ucsf.edu/chimerax/">https://www.cgl.ucsf.edu/chimerax/</a>
Phenix	<a href="#">Adams et al. (2010)</a>	<a href="https://www.phenix-online.org/">https://www.phenix-online.org/</a>
Coot	<a href="#">Emsley et al. (2010)</a>	<a href="https://www2.mrc-lmb.cam.ac.uk/">https://www2.mrc-lmb.cam.ac.uk/</a>

(Continued on next page)

### Continued

REAGENT or RESOURCE	SOURCE	IDENTIFIER
Pymol	PyMOL Molecular Graphics System, Version 2.0 Schrödinger	<a href="https://pymol.org/2/">https://pymol.org/2/</a>
Illustrator	Adobe	N/A
Other		
Quantifoil grid (Au, 300 mesh, R1.2/1.3)	Quantifoil Micro Tools GmbH	Cat# Q62307
Superose 6 10/300 Increase GL	GE Healthcare Life Sciences	Cat# 29091596

### RESOURCE AVAILABILITY

#### Lead contact

Further information and requests for resources and reagents should be directed to and will be fulfilled by the lead contact, Yongqun Zhu ([zhuyongqun@zju.edu.cn](mailto:zhuyongqun@zju.edu.cn)).

#### Materials availability

Materials generated in this study will be made available on request and might require a material transfer agreement.

#### Data and code availability

- The cryo-EM map and coordinates have been deposited in the Electron Microscopy Data Bank and Protein Data Bank under accession numbers PDB: 7WLY and EMBD: EMD-32594 (Omicron S-ECD-35B5 Fab [1 down- and 2 up-RBDs]), PDB: 7WLZ and EMBD: EMD-32595 (Omicron S-ECD-35B5 Fab [1 up-, 1 down-, and 1 invisible up-RBD]), and PDB: 7WM0 and EMBD: EMD-32596 (Omicron RBD-35B5 Fab [local refinement]).
- This paper does not report any original code.
- Any additional information required for reanalyzing the data reported in this work paper is available from the lead contact upon request.

### EXPERIMENTAL MODEL AND SUBJECT DETAILS

#### Cell lines

HEK293F cells (Thermo Fisher Scientific, Cat# 11625019) were cultured in the serum free SMM 293-TI medium (Sino Biological) at 37°C with 8% CO<sub>2</sub> on an orbital shaker platform. ExpiCHO-S cells (Thermo Fisher Scientific, Cat# A29133) were cultured in the ExpiCHO expression medium (Thermo Fisher Scientific) at 37°C with 8% CO<sub>2</sub> on an orbital shaker platform. Human ACE2-expressing HEK-293T (293T/ACE2) cells were provided by Dr. Zhaohui Qian (Chinese Academy of Medical Sciences and Peking Union Medical College) and were maintained in Dulbecco's Modified Essential Medium (DMEM) supplemented with 10% fetal bovine serum (FBS) and 1% penicillin-streptomycin at 37°C in a 5% CO<sub>2</sub> setting. VeroE6-TMPRSS2 cells (JCRB, Cat# JCRB1819) were cultured in DMEM containing 10% FBS, 2 mM L-glutamine, and 100 U/mL/mL penicillin and incubated at 37°C in a 5% CO<sub>2</sub> setting.

#### Virus strains

SARS-CoV-2 pseudoviruses carrying the Luciferase reporter gene were purchased from the Sino Biological. The catalog numbers of the WT, Delta, and Omicron pseudoviruses are PSV001, PSV011, and PSV016, respectively. The Delta pseudovirus contains the following mutations: T19R, G142D, E156G, del157/158, L452R, T478K, D614G, P681R, and D950N. The Omicron pseudovirus contains the following mutations: A67V, H69del, V70del, T95I, G142D, V143del, Y144del, Y145del, N211del, L212I, ins214EPE, G339D, S371L, S373P, S375F, K417N, N440K, G446S, S477N, T478K, E484A, Q493R, G496S, Q498R, N501Y, Y505H, T547K, D614G, H655Y, N679K, P681H, N764K, D796Y, N856K, Q954H, N969K, and L981F. The authentic SARS-CoV-2 Omicron strain hCoV-19/Hong Kong/HKU-691/2021 (HKU691) (GISAID accession number EPI\_ISL\_7138045) was isolated from the combined nasopharyngeal-throat swabs of 2 people with COVID-19 in Hong Kong and was further cultured and titrated by plaque assays using VeroE6-TMPRSS2 cells.

### METHOD DETAILS

#### Monoclonal antibody

Monoclonal antibody was produced by using the ExpiCHO Expression System (Thermo Fisher Scientific). In brief, ExpiCHO-S cells were transfected with master mixture containing 200 µg heavy chain plasmid, 200 µg light chain plasmid and 640 µL ExpiFectamine

CHO reagent. On the next day post-transfection, cultured cells were added with ExpiCHO enhancer and ExpiCHO feed. On day 5 post-transfection, another volume of ExpiCHO feed was added into cultured cells. On day 12 post-transfection, supernatants were harvested for antibody purification by using rProtein A Sepharose affinity chromatography (Sigma).

### ELISA

Each well of the ELISA plates was coated with 50 ng of SARS-CoV-2 WT S trimer protein (Acro Biosystems, SPN-C52H7) or Delta S protein (Sino Biological, 40589-V08H10) or Omicron S protein (Acro Biosystems, SPN-C52Hz) in 100  $\mu$ L PBS overnight at 4°C. On the following day, the ELISA plates were incubated with blocking buffer (5% FBS + 0.1% Tween 20 in PBS) for 1 h. Then, serially diluted mAbs were added to the plates and incubated for 1 h. After washing with PBST (PBS + 0.1% Tween 20), the plates were incubated with HRP-conjugated anti-human IgG antibody (Bioss Biotech) for 30 min, followed by washing with PBST and addition of TMB (Beyotime). The ELISA plates were allowed to react for  $\sim$ 5 min and then stopped by 1 M H<sub>2</sub>SO<sub>4</sub> stop buffer. The optical density (OD) value was determined at 450 nm. The EC<sub>50</sub> (concentration for 50% of maximal effect) values were calculated by using nonlinear regression in GraphPad version 6.0.

### SARS-CoV-2 pseudovirus neutralization

Human ACE2-expressing HEK-293T (293T/ACE2) cells were seeded into 96-well plates (Corning, 3599) at a density of 20,000 cells per well. The next day, mAbs were serially diluted in complete media, mixed with WT pseudoviruses (Sino Biological, PSV001) or Delta pseudoviruses (Sino Biological, PSV011) or Omicron pseudoviruses (Sino Biological, PSV016) and incubated for 1 h at 37°C. Then, culture media of 293T/ACE2 cells was replaced by pre-incubated mAb/pseudovirus mixture and the cells were cultured for another 16 h. Next, 293T/ACE2 cells were cultured with fresh complete media for an additional 24 h and the luciferase activity of SARS-CoV-2 pseudovirus-infected 293T/ACE2 cells were measured by a luciferase reporter assay kit (Promega, E1910). The IC<sub>50</sub> (50% inhibitory concentration) values were calculated by fitting a non-linear four-parameter dose-response curve in GraphPad version 6.0.

### Authentic SARS-CoV-2 Omicron neutralization

The Omicron variant strain HKU691 was used for authentic viral neutralization assay. The virus titration was done by plaque assay using TMPRSS2-expressing Vero E6 cells. Authentic SARS-CoV-2 neutralization assay was performed according to previous studies (Wang et al., 2021; Zhou et al., 2021). In brief, Vero E6 cells were seeded in a 24-well culture plates at a density of  $2 \times 10^4$  cells per well at 37 °C for 24 h. Then, authentic SARS-CoV-2 Omicron (MOI = 0.005) and 5-fold serially diluted 35B5 mAbs (from 25  $\mu$ g/mL to 0.00032  $\mu$ g/mL) were mixed in the medium with 2% FBS, and were then added into the Vero E6 cells. The culture supernatant of 48 h post-infection was collected to detect target gene RdRp/Hel by qRT-PCR. Forward primer (RdRp/Hel): 5'-CGCATACAGTCTTR CAGGCT-3'; reverse primer (RdRp/Hel): 5'-GTGTGATGTTGAWATGACATGGTC-3'. IC<sub>50</sub> values were determined by fitting a non-linear four-parameter dose-response curve in GraphPad version 6.0.

### Production and purification of Omicron S-ECD and 35B5 Fab proteins

The Omicron S-ECD gene were cloned using the overlapping PCR method from the plasmid encoding the ectodomains of the SARS-CoV-2 S-6P (HexoPro) mutant, which was kindly provided by Dr. Junyu Xiao of Peking University. HEK293F cells were cultured in the SMM 293-TI medium (Sino Biological) at 37°C with 8% CO<sub>2</sub>. The Omicron S-ECD-containing plasmid was transiently transfected into HEK293F cells using 40-kDa linear polyethylenimine (PEI) (Polysciences) with the PEI/DNA mass ratio of 3:1 and 1 mg DNA for per liter of culture when the cell density reached  $2 \times 10^6$  cells per mL. At day 4 post-transfection, the supernatants of the cell culture were harvested by centrifugation at 10,000  $\times$  g for 30 min followed by buffer-exchange by sartorius VIVAFLow 200 cassette with a molecular weight cutoff of 30 kDa. The secreted Omicron S-ECD protein was purified using HisPur cobalt resins (Thermo Fisher Scientific). Further purification was carried out using size-exclusion chromatography with a Superose 6 10/300 column (GE Healthcare) in the buffer containing 20 mM HEPES (pH 7.2), 150 mM NaCl, and 10% Trehalose. The Fab region of the 35B5 was obtained after the digestion by papain for 40 min at 37°C in a buffer containing 20 mM HEPES pH 7.2, 150 mM NaCl, 5 mM EDTA and 5 mM L-cysteine. The obtained 35B5 Fab was purified with a Desalting column (GE Healthcare Life Sciences) to remove L-cysteine, and then further purified in a HiTrap Q column (GE Healthcare Life Sciences). The purified Fabs were collected and concentrated to 0.6 mg/mL.

### Differential scanning fluorimetry

The S-ECD HexaPro proteins of Omicron and G614 SARS-CoV-2 were diluted in the dilution buffer of 20 mM HEPES, pH 7.2, and 150 mM NaCl to 0.2 mg/mL. The 5000 $\times$  SYPRO Orange (Sigma) was diluted to 50 $\times$  using the above dilution buffer. In a 96-well qPCR white plate (Bio-Rad), 18  $\mu$ L protein or dilution buffer (negative control) and 2  $\mu$ L dye were mixed together in each well and incubated for 20 min in dark at room temperature. In a Bio-Rad CFX96 real-time PCR instrument, fluorescence signals were measured every temperature ramp cycle (0.6°C in 10 s) from 25°C to 95°C. Data was plotted as the negative first derivative of the relative fluorescence unit (RFU) as a function of temperature by the Bio-Rad CFX Maestro software. Three parallel measurements were performed for each sample and one representative plot was shown.

### Negative-staining analysis

For negative-staining assays, Omicron S-ECD and 35B5 Fab proteins were diluted in the buffer of 20 mM HEPES, pH 7.2, and 150 mM NaCl to 0.02 mg/mL and 0.04 mg/mL, respectively. 2  $\mu$ L of 35B5 Fab was mixed with 2  $\mu$ L Omicron S-ECD and incubated on ice for 3 min. The samples were loaded in the glow-discharged carbon-coated copper grids and stained with 3% Uranyl Acetate (UA). The prepared grids were examined using a transmission electron microscope (HITACHI) operated at 80 kV. Micrographs were recorded using a GATAN camera with 120,000 $\times$  nominal magnification.

### Cryo-EM sample preparation and data collection

2  $\mu$ L of Omicron S-ECD protein (1.2 mg/mL) and 2  $\mu$ L of 35B5 Fab (0.6 mg/mL) were incubated for 20 s at room temperature and then immediately loaded onto the glow-discharged holey-carbon gold grids (Quantifoil, R1.2/1.3). The grids were washed using the buffer containing 20 mM HEPES, pH 7.2, 150 mM NaCl and 4% Trehalose. The washed grids were blotted using a Mark IV Vitrobot (Thermo Fisher Scientific) at 100% humidity, 22°C and blot force  $-3$  (TED PELLA 595 filter paper) for 3 s, and submerged in liquid ethane by plunge-freezing. The micrographs were recorded on a FEI Titan Krios (Thermo Fisher Scientific) electron microscope operated at 300 kV. Totally, 7678 movies were recorded on a K2 Summit direct electron detector (Gatan) in the counting mode (1.014 Å/pixel) by the serialEM software at a nominal magnification of 29,000 using a defocus range of 1.0–1.3  $\mu$ m (Mastrorade, 2005). The micrographs were dose-fractionated into 32 frames with a total electron exposure of  $\sim 64$  electrons per Å<sup>2</sup>.

### Cryo-EM image processing

Raw movie frames were binned, aligned and averaged into motion-corrected summed images using MotionCor2 (Zheng et al., 2017). The dose-weighted images were then imported into cryoSPARC for the following image processing, including CTF estimation, particle picking and extraction, 2D classification, ab initio 3D reconstruction, heterogeneous 3D refinement and non-uniform homogeneous refinement (Punjani et al., 2017). Four representative particle templates were generated in 2D classification of 74,593 particles auto-picked by the blob picker from 1000 micrographs. Using these templates, 2,749,814 particles were extracted with a box size of 386  $\times$  386 and classified into 150 classes in 2D classification. Among them, 45 classes that included 669,842 particles were selected for ab initio 3D reconstruction and heterogeneous refinement. Finally, 556,976 particles reconstructed an apparent architecture of the Omicron S-ECD-35B5 Fab complex and were subjected to two more rounds of ab initio 3D reconstruction and heterogeneous refinement before non-uniform refinement. Then the particles generated two abundant populations of the Omicron S-ECD-35B5 Fab complex reconstructions. Local refinements of the RBD-35B5 Fab region were performed to improve the interface density in cryoSPARC. Sharpened maps were generated and validated for model building and refinement. Reported resolutions are based on the gold-standard Fourier shell correlation of 0.143 criterion.

### Cryo-EM structure modeling and analysis

All model building was performed in Coot (Emsley et al., 2010). The structures of S-ECD and 35B5 Fab in our previously determined structure of the WT S-ECD-35B5 Fab complex were used as initial models in the model building of the Omicron S-ECD-35B5 Fab complex. Structural refinement and validation were carried out in Phenix (Adams et al., 2010). Structural figures were prepared using UCSF ChimeraX version 1.2 (Goddard et al., 2018).

### QUANTIFICATION AND STATISTICAL ANALYSIS

The statistical analyses were performed in GraphPad version 6.0 unless otherwise mentioned. In the ELISA assay, the mean values  $\pm$  SEM for three independent experiments were plotted and the EC<sub>50</sub> values were calculated by using sigmoidal dose-response nonlinear regression (Figure 1A). In neutralization assays, the mean values  $\pm$  SEM for three (Figure 1C) or two (Figure 1D) independent experiments were plotted and the IC<sub>50</sub> values were calculated by fitting a non-linear four-parameter dose-response curve. In the differential scanning fluorimetry assay, the melting temperatures (T<sub>m</sub>) are shown as mean  $\pm$  SD for three independent measurements and one representative plot was drawn using the Origin 9.0 software (Figure S2G). No methods were used to determine whether the data met assumptions of the statistical approach as no statistical tests were performed in this study.